# COMPUTATIONALLY-EFFICIENT BANDWISE GBM MODEL FOR HYPERSPECTRAL NONLINEAR UNMIXING

*Touseef Ahmad*[⋆,†], *Soumyendu Raha*[†], *Rosly B Lyngdoh* [⋆], *Anand S S*[⋆], Praveen K Gupta[⋆], and Arundhati Misra[⋆]

[⋆]Space Applications Centre Ahmedabad, Indian Space Research Organization, India
[†]Department of Computational and Data Sciences, Indian Institute of Science Bangalore, India

## ABSTRACT

Nonlinear Unmixing using the Band-wise Generalized Bilinear Mixing (NU-BGBM) model specifies an acceptable mixing scenario up to the second-order interaction of light rays and also suppresses various types of mixed noise while performing unmixing. However, NU-BGBM requires high computational time and multiple parameter tuning, which could practically limit its application to large HyperSpectral Images (HSIs). In this context, we propose a computationally efficient BGBM as a fast and robust variant of the NU-BGBM method, In this model, the objective function for the non-linear optimization scheme is designed without the sparsity constraint, and an iterative scheme based on the Alternating Direction Method of Multipliers (ADMM) is formulated for solving the proposed model. Extensive analyses have been carried out on synthetic (with simulated mixed noise) and real HSIs. The performance of the proposed method was compared with the NU-BGBM model using signal-to-reconstruction error (SRE), abundance Root-Mean-Square Error (aRMSE), source Root-Mean-Square Error (sRMSE), and Root-Sum-Squared (RSS) error. Results from extensive numerical analysis reveal that the proposed method reduces computation time (on an average six times faster) while being comparable (and often better) than NU-BGBM in terms of accuracy on large data sets.

***Index Terms***— Hyperspectral image unmixing, bandwise GBM, ADMM.

## I. INTRODUCTION

In HyperSpectral Images (HSIs), the multiple interactions of light rays among the neighbouring substances introduce nonlinearity and hamper the performance of linear-mixture model (LMM). Physics-inspired models such as the bilinear mixing model (BLM) [1], multilinear mixing model [2], and intimate mixture model [3] are used for nonlinear unmixing analysis. Among them, the generalised bilinear mixing (GBM) model [4] handles light ray interactions with materials up to the second order at each pixel of the HSI. However, higher-order interactions are neglected in this model. Higher-order interactions have minor contributions to improve the unmixing accuracy and also involve large-scale optimization problems [4].

Most GBM-based spectral unmixing methods are designed for Gaussian noise, with the premise that Gaussian noise intensities stay constant across all HSI channels. However, in real scenario, the HSI contains varying Additive White Gaussian Noise (AWGN) levels in all bands. Similarly, various forms of noise, such as impulse noise, dead pixels, lines, stripes, and so on, also deteriorate HSI. Aggarwal et al. [5] presented a spectral unmixing approach for HSI in the presence of mixed noise that uses joint-sparsity and total variation spatial regularisation and can account for several forms of noise. However, it is incapable of accounting for the multiple interactions of light rays (nonlinear interactions). Li et al. [6] recently presented a nonlinear unmixing technique based on bandwise GBM that assumed distinct AWGN at various HSI bands as well as a sparsity constraint on noise terms. The sparsity constraint on the noise component, on the other hand, makes this approach computationally expensive for large-scale spectral unmixing problems. In this context, we propose an augmented bandwise GBM for nonlinear hyperspectral unmixing analysis, which is named as NU-RBGBM i.e. the nonlinear unmixing using robust bandwise generalized bilinear mixing model. This model is provided within the maximum a posteriori (MAP) paradigm [6], which assumes complex mixed noise in actual HSI, i.e each band of HSI is contaminated by mixed noise, and the AWGN across the bands is considered to be varied. Other noise types, such as dead pixels or lines, impulse noise, and stripes, typically exhibit sparseness characteristics (affecting a small part of the HSI). The Alternating Direction Method of Multipliers (ADMM) [7] was formulated to solve the proposed model. Because no constraint is applied to the abundance matrix, no extra parameters in the proposed technique need to be adjusted to improve precision. Accuracy assessment was performed using signal-to-reconstruction error (SRE), abundance root-mean-square error (aRMSE), source root-mean-square error (sRMSE), and root-sum-squared (RSS) measures [6], [8]. Extensive numerical analysis using simulated (with mixed noise) and real datasets demonstrated the effectiveness of the proposed method.

## II. BANDWISE GENERALIZED BILINEAR MIXING MODEL

Existing unmixing techniques based on GBM are assumed to contain the same white Gaussian noise for each band of HSI. However, atmospheric effects, instrumental (sensor) noise, shot (photon) noise, impulse noise, dead pixels or lines, and strips are all familiar sources of noise that degrade real HSIs [9]. The noise in HSI can also be classified into two classes, i.e. dense noise and sparse noise. All pixels of HSI are contaminated by dense noise. However, sparse noise affects only a small number of pixels. As a result, a robust GBM model for $L$ channels, $M$ endmembers, and $P$ samples can be written as [6]:

$$\mathbf{Z} = \mathbf{AX} + \mathbf{BY} + \mathbf{S} + \mathbf{N}, \tag{1}$$

where $\mathbf{Z} \in \mathbb{R}^{L\times P}$ is hyperspectral data matrix, $\mathbf{A} \in \mathbb{R}^{L\times M}$, is the endmember matrix and $\mathbf{X} \in \mathbb{R}^{M\times P}$, corresponding abundance matrix. $\mathbf{B} = [\mathbf{a_1} \odot \mathbf{a_2}, ..., \mathbf{a_{M-1}} \odot \mathbf{a_M}] \in \mathbb{R}^{L\times M(M-1)/2}$ is the bilinear endmember interaction matrix ($\mathbf{a_i}$ denotes $i^{th}$ endmember), $\mathbf{Y} = [\mathbf{y_1}, ..., \mathbf{y_P}] \in \mathbb{R}^{M(M-1)/2\times P}$ is corresponding bilinear abundance matrix. Here, $\mathbf{S}$ & $\mathbf{N} \in \mathbb{R}^{L\times P}$ denote sparse and dense noise respectively[6]. Abundance Non-negativity Constraint (ANC) and Abundance Sum-to-one Constraint (ASC) were assumed over abundance coefficients. However, ASC may not satisfy for all pixels due to the signature variability within the HSI [10], therefore, ASC is avoided in the proposed method. Thus, the required constraints for GBM can be defined as follows:

$$\mathbf{X} \geq \mathbf{0} \ \ \& \ \ \mathbf{0} \leq \mathbf{Y} \leq \mathbf{Y}^*, \tag{2}$$

where matrix $\mathbf{X} \geq \mathbf{0}$ means $\mathbf{X(i,j)} \geq \mathbf{0}$, $\forall \mathbf{i,j}$. $\mathbf{Y}$ is bounded by some matrix such as $\mathbf{Y}^*_{\mathbf{(i,j),q}} = \mathbf{X_{i,q}X_{j,q}}$, $(q = 1, 2, ..., P)$.

A weighted diagonal matrix $\mathbf{W} \in \mathbb{R}^{L \times L}$ is introduced in data fidelity term for spectral unmixing using bandwise GBM [6], in which diagonal elements are estimated as $\mathbf{W}_{i,i} = \frac{1}{\sigma_i}(i = 1, ..., L)$ ($\sigma_i^2$ represent the variance of Gaussian noise in $i^{th}$ band). As the band's weight decreases, the AWGN variance increases. It indicates that the weighting factor can have varying AWGN intensities in different HSI bands [11]. For generating weighting matrix $\mathbf{W}$, the noise was estimated using the hyperspectral signal identification by minimum error (HySime) [12] algorithm. Extensive simulations over simulated datasets have revealed that the effect of the sparse noise term $\mathbf{S}$ in Eq. (1) is negligible, this term was removed from the formulation for the proposed unmixing scheme.

## III. ADMM FORMULATION FOR THE PROPOSED NU-RBGBM

Constrained optimization problem for robust bandwise-GBM can be written as follows:

$$\min_{\mathbf{X},\mathbf{Y}} \frac{1}{2} \|\mathbf{W}(\mathbf{Z} - \mathbf{AX} - \mathbf{BY})\|_F^2 \quad \text{s.t. } \mathbf{X} \geq \mathbf{0}, \mathbf{0} \leq \mathbf{Y} \leq \mathbf{Y}^*. \tag{3}$$

The ADMM (for more details see Boyd's et al. [13]) has been actively designed to solve constraint optimization problems. Thus above Eq. (3) can be reformulated as follows:

$$\arg\min_{\mathbf{X},\mathbf{Y}} \frac{1}{2} \|\mathbf{W}(\mathbf{Z} - \mathbf{AX} - \mathbf{BY})\|_F^2 + \iota_{\mathbb{R}+}(\mathbf{X}) + \iota_{\mathbb{R}_{\mathbf{bound}}}(\mathbf{Y}) \tag{4}$$

where $\iota_{\mathbb{R}+}(\mathbf{X}) = \sum_{i,j} \iota_{\mathbb{R}+}(X_{i,j})$ is the indicator function for the non-negative orthant $\mathbb{R}_+$, $X_{i,j}$ is the $(i,j)th$ element of $\mathbf{X}$, and $\iota_{\mathbb{R}+}(X_{i,j})$ is zero when $X_{i,j}$ belongs to the non-negative orthant and $+\infty$ otherwise. $\iota_{\mathbb{R}_{bound}}(\mathbf{Y}) = \sum_{i,j} \iota_{\mathbb{R}_{bound}}(\mathbf{Y}_{i,j})$ , denotes the indicator function for the bounded interval $[\mathbf{0}, \mathbf{Y}^*]$, i.e.

$$\iota_{\mathbb{R}_{bound}}(\mathbf{Y_{i,j}}) = \begin{cases} 0, & \text{if } X_{i,j} \in [\mathbf{0}, \mathbf{Y^*_{i,j}}] \\ +\infty, & \text{Otherwise.} \end{cases}$$

The above problem defined in Equation (4) can be reformulated using Douglas–Rachford splitting method [14] as:

$$\min_{\mathbf{X},\mathbf{Y},\mathbf{V_1},\mathbf{V_2}} \frac{1}{2} \|\mathbf{W}(\mathbf{Z} - \mathbf{AX} - \mathbf{BY})\|_F^2 + \iota_{\mathbb{R}+}(\mathbf{V_1}) + \iota_{\mathbb{R}_{bound}}(\mathbf{V_2}) \quad \text{subject to} \quad \mathbf{V_1} = \mathbf{X}, \mathbf{V_2} = \mathbf{Y}, \tag{5}$$

where $\mathbf{V_1}$ & $\mathbf{V_2}$ are introduced as auxiliary variables for the optimization problem. Above equation can be written in the compact form as:

$$\min_{\mathbf{V},\mathbf{Q}} \mathbf{g}(\mathbf{V}, \mathbf{Q}), \quad s.t. \quad \mathbf{GQ} + \mathbf{HV} = \mathbf{O}, \tag{6}$$

where

$$\mathbf{g}(\mathbf{V}, \mathbf{Q}) = \frac{1}{2} \|\mathbf{W}(\mathbf{Z} - \mathbf{AX} - \mathbf{BY})\|_F^2 + \iota_{\mathbb{R}+}(\mathbf{V_1}) + \iota_{\mathbb{R}_{\mathbf{bound}}}(\mathbf{V_2}),$$

$$\mathbf{G} = \begin{bmatrix} \mathbf{I} & 0 \\ 0 & \mathbf{I} \end{bmatrix}, \mathbf{H} = \begin{bmatrix} -\mathbf{I} & 0 \\ 0 & -\mathbf{I} \end{bmatrix}, \mathbf{V} = [\mathbf{V_1}\ \mathbf{V_2}]^T,$$

$\mathbf{Q} = [\mathbf{X}\ \mathbf{Y}]^T$, $\mathbf{O} = [\mathbf{0}\ \mathbf{0}]^T$.

The augmented Lagrangian function for the problem in Equation (6) can be written as

$$\mathfrak{L}(\mathbf{V}, \mathbf{Q}, \mathbf{D}) = \mathbf{g}(\mathbf{V}, \mathbf{Q}) + \frac{\mu}{\mathbf{2}} \|\mathbf{GQ} + \mathbf{HV} - \mathbf{O} - \mathbf{D}\|_\mathbf{F}^\mathbf{2}, \tag{7}$$

where $\mu > 0$ is positive constant (penalty parameter) and $\frac{\mathbf{D}}{\mu}$ denotes the Lagrange multipliers which are associated to the constraint $\mathbf{GQ} + \mathbf{HV} = \mathbf{O}$. Therefore, we can sequentially optimize the Lagrangian function $\mathfrak{L}$ with respect to $\mathbf{V}$, $\mathbf{Q}$ and $\mathbf{D}$, also main optimization problem can be split into sub-problems and solved individually. Thus, the pseudo code for solving the constrained optimization problem in Eq.(6) has been described in Algorithm-1. For convergence and stability analysis, Ahmad et al.[8] can be referred.

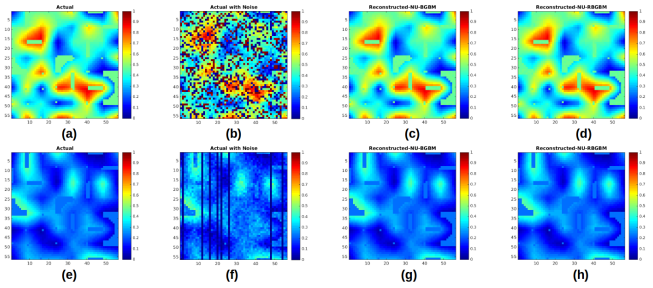


**Fig. 1**: The actual Band-70, the Band-70 with mixed noise, reconstructed using NU-BGBM, and reconstructed using NU-RBGBM are presented in (a), (b), (c), and (d), respectively. In (e), (f), (g), and (h), the actual Band-125, Band-125 with mixed noise, reconstructed using NU-BGBM, and reconstructed using NU-RBGBM are displayed, respectively.

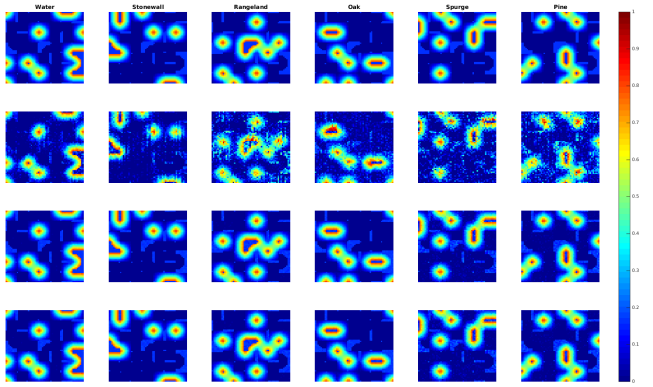


**Fig. 2**: Results obtained in simulated data experiment: Actual abundance (1st row), FCLS (2nd row), NU-BGBM (3rd row) and NU-RBGBM (last row).

**Algorithm 1: Pseudo-code for NU-RBGBM**

**Input:** $\mathbf{Z}, \mathbf{A}, \mathbf{B}, \mu$
**Output:** $\mathbf{X}, \mathbf{Y}$
**Initialization:** $\mathbf{W}, \mathbf{X}, \mathbf{Y}, \mathbf{V_1}, \mathbf{V_2}, \mathbf{D_1}, \mathbf{D_2}$**, for k=0**
**While not converged Do**
$\mathbf{X^{k+1}} = [(\mathbf{WA})^\mathbf{T}(\mathbf{WA}) + \mu\mathbf{I}]^{-1}[(\mathbf{WA})^\mathbf{T}\mathbf{W}(\mathbf{Z} - \mathbf{BY^k}) + \mu(\mathbf{V_1^k} - \mathbf{D_1^k})]$;
$\mathbf{Y^{k+1}} = [(\mathbf{WB})^\mathbf{T}(\mathbf{WB}) + \mu\mathbf{I}]^{-1}[(\mathbf{WB})^\mathbf{T}\mathbf{W}(\mathbf{Z} - \mathbf{AX^{k+1}}) + \mu(\mathbf{V_2^k} - \mathbf{D_2^k})]$;
$\mathbf{V_1^{k+1}} = \mathbf{max}(\mathbf{X^{k+1}} + \mathbf{D_1^k}, \mathbf{0})$;
$\mathbf{V_2^{k+1}} = \mathbf{min}(\mathbf{max}(\mathbf{Y^{k+1}} + \mathbf{D_2^k}, \mathbf{0}), \mathbf{Y^*})$;
$\mathbf{D_1^{k+1}} = \mathbf{D_1^k} - (\mathbf{V_1^{k+1}} - \mathbf{X^{k+1}})$
$\mathbf{D_2^{k+1}} = \mathbf{D_2^k} - (\mathbf{V_2^{k+1}} - \mathbf{Y^{k+1}})$
**Update k: k=k+1**
**end while : Some stopping criteria[8].**
**Return:** $\mathbf{X} = \mathbf{X^{k+1}}, \mathbf{Y} = \mathbf{Y^{k+1}}$.

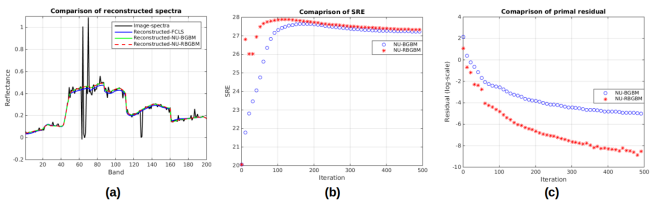


**Fig. 3**: Comparison of the reconstructed spectra at random pixel (a), SRE (b), and primal residual at log scale (c).

## IV. EXPERIMENTAL ANALYSIS OVER SIMULATED AND REAL DATASETS

In this section, the performance of the proposed algorithm is compared with FCLS and NU-BGBM algorithms. In Li et al. [6], NU-BGBM algorithm was compared with FCLS[15], GDA [1], Semi-NMF [16], and BPOGM [17] and reported that NU-BGBM algorithm outperformed (refer [6] for more details). FCLS is based on LMM, and all other methods are based on GBM. Due to trivial comparisons as discussed in [6], we considered only FCLS (LMM) and NU-BGBM to discuss the performance of NU-RBGBM in this study.

We have adopted the recommended default parameters as mentioned in [6] for a fair comparison of the proposed algorithm. There are mainly four parameters such as the regularization parameter $\lambda$, the Lagrange multiplier $\mu$, the error tolerance $\epsilon$, and the maximum number of iterations $I$. In the entire experimental analysis, we have fixed the parameters $\mu = 0.01$, $\epsilon = 10^{-6}$ , $I = 500$. Accuracy measures such as SRE, aRMSE , sRMSE and computation time ( for more details [8]) were employed to evaluate the performance. All simulated and real HSI experiments were carried out on a Windows-10 computer with i7-processor and 8GB RAM.

### IV-A. Experiment-1:Simulated Dataset

Experiments were designed to simulate the mixed complex noise in simulated HSIs (For more details refer[6]). Individual and combination of all three types of noises (Gaussian, impulse and deadlines). We use FCLS, NU-BGBM, and NU-RBGBM to unmix the synthetic HSIs using the selected endmembers. All seven simulated datasets correspond to different noise types have been compared and displayed in Table I, which shows that the proposed algorithm is either performing better than or at par with NU-BGBM (for $\lambda = 10^{-2}$) in terms of SRE, aRMSE and sRMSE. Moreover, NU-RBGBM was computationally efficient than NU-BGBM in all seven cases.

Reconstructed HSIs obtained from NU-BGBM and NU-RBGBM are also compared with actual and noisy data cubes. Figure 1 shows the actual Band-70 and Band-125 images and their reconstructed versions obtained from NU-BGBM and NU-RBGBM. From visual inspection, it can be noticed that mixed types of noises such as Gaussian, impulse, and dead-lines were removed by NU-RBGBM, and also the performance was at par with the NU-BGBM algorithm with less computational time. Estimated abundance maps corresponding to each endmember are displayed in Fig. 2. The first row shows actual abundance maps, and the remaining rows show the estimated abundance maps obtained from FCLS, NU-BGBM, and NU-RBGBM, respectively, which shows that the results obtained from NU-RBGBM were much the same as NU-BGBM with minimum computational cost. The spectra of a random pixel in reconstructed HSI using FCLS, NU-BGBM, and NU-RBGBM are compared with their respective spectra in the actual imagery and plotted in Fig. 3(a), which indicates the similar performances of both NU-RBGBM and NU-BGBM. SRE and primal residual(log-scale) are estimated and compared in each iteration for NU-BGBM and NU-RBGBM and displayed in Fig. 3(b) and 3(c) respectively,

**Table I**: Accuracy Assessment of the unmixing results over synthetic and real datasets with 500 iterations.

| Type of Noise | Acc. Asses. | FCLS | NU-BGBM | NU-RBGBM |
|---|---|---|---|---|
| Gaussian Noise | SRE (dB) | 12.5743 | 29.0253 | 28.9970 |
| | aRMSE | 0.0620 | 0.0093 | 0.0094 |
| | sRMSE | 0.0296 | 0.0298 | 0.0298 |
| | Time(in Sec.) | 0.8862 | 24.7044 | 3.6960 |
| Impulse Noise | SRE (dB) | 12.7707 | 26.4258 | 26.7181 |
| | aRMSE | 0.0109 | 0.0126 | 0.0122 |
| | sRMSE | 0.0662 | 0.0671 | 0.0671 |
| | Time(in Sec.) | 0.8430 | 25.0998 | 3.1514 |
| Dead-lines | SRE (dB) | 12.5202 | 28.4889 | 30.5453 |
| | aRMSE | 0.0624 | 0.0099 | 0.0078 |
| | sRMSE | 0.0209 | 0.0211 | 0.0211 |
| | Time(in Sec.) | 0.8659 | 25.2469 | 3.3085 |
| Gaussian+Impulse | SRE (dB) | 10.6499 | 28.9148 | 28.8906 |
| | aRMSE | 0.0774 | 0.0094 | 0.0095 |
| | sRMSE | 0.0725 | 0.0734 | 0.0734 |
| | Time(in Sec.) | 0.8776 | 25.6672 | 3.2737 |
| Gaussian+Dead-lines | SRE (dB) | 10.5607 | 28.7439 | 28.7169 |
| | aRMSE | 0.0782 | 0.0096 | 0.0097 |
| | sRMSE | 0.0362 | 0.0366 | 0.0366 |
| | Time(in Sec.) | 0.9043 | 26.8656 | 3.4142 |
| Impulse +Dead-lines | SRE (dB) | 10.9681 | 25.1396 | 25.4025 |
| | aRMSE | 0.0746 | 0.0146 | 0.0142 |
| | sRMSE | 0.0694 | 0.0703 | 0.0703 |
| | Time(in Sec.) | 0.8306 | 24.9464 | 3.3843 |
| Gaussian+Impulse +Dead-lines | SRE (dB) | 9.5409 | 28.6274 | 28.6214 |
| | aRMSE | 0.0879 | 0.0098 | 0.0098 |
| | sRMSE | 0.0754 | 0.0764 | 0.0764 |
| | Time(in Sec.) | 0.9011 | 25.1605 | 3.4699 |
| Real HSI(Jasper-Ridge) | sRMSE | 0.043255 | 0.018331 | 0.018234 |
| | Time(in Sec.) | 5.199167 | 96.839919 | 13.893458 |

which indicates the superiority of the proposed algorithm over NU-BGBM.

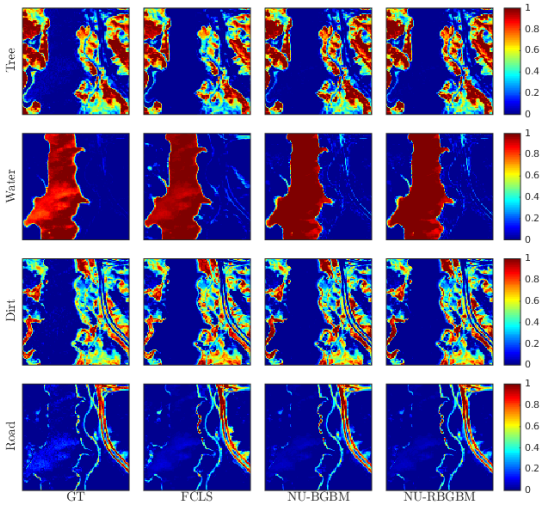


**Fig. 4**: Results obtained in real dataset experiment (AVIRIS:Jasper-Ridge) are displayed as ground truth [18](1st Column), estimated abundance maps using FCLS , NU-BGBM and NU-RBGBM are given in 2nd, 3rd and 4th columns respectively.

### IV-B. Experiment-2: Real Data Dataset (AVIRIS:Jasper-Ridge)

In this experiment, the AVIRIS Jasper-Ridge HSI was examined for performance evaluation of the proposed algorithm. The Vertex Component Analysis (VCA) [19] was used for endmember extraction, which was identified as Tree, Water, Soil, and Road respectively. Since actual abundances in real datasets are unknown, and we cannot compute SRE and aRMSE for comparison, sRMSE was employed to evaluate the unmixing performance of different methods. Estimated abundance maps using FCLS, NU-BGBM, and NU-RBGBM are displayed in Fig. 4, which shows that NU-RBGBM performs significantly better than other state-of-the-art

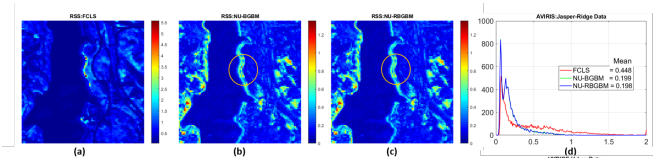


**Fig. 5**: RSS error maps generated using FCLS(a), NU-BGBM(b), NU-RBGBM(c) with histogram comparison(d) over AVIRIS:Jasper-Ridge dataset. The yellow circle highlights region with high RSS values for NU-BGBM as compared to NU-RBGBM.

methods. sRMSE and computation time were also estimated and displayed in the last row of Table I, which also denotes the superiority of the proposed method.

The RSS error maps obtained from FCLS, NU-BGBM, and NU-RBGBM are depicted in Fig. 5. Pixels with the highest RSS ($RSS_{max}$) intensities were observed on the RSS map of FCLS($RSS_{max} \simeq 5.5$), which is very high as compared to NU-BGBM and NU-RBGBM ($RSS_{max} \simeq 1.2$). The very high RSS values of FCLS can be attributed to the non-linear interactions of electromagnetic radiation in the real datasets, which FCLS could not approximate. The yellow circle (in Fig. 5(b) and 5(c)) highlights the region with high RSS values for NU-BGBM as compared to NU-RBGBM. The histograms (with mean values) further confirm this in Fig. 5(d), which illustrates the distribution of RSS values over real HSIs. The frequency of occurrence of RSS values above 0.25 was high in the RSS map of FCLS as compared to other algorithms. Last row of Table I shows that the proposed NU-RBGBM can obtain the best sRMSE and less computation time for AVIRIS: Jasper-Ridge (sRMSE = 0.01823, Time = 13.8935) and as compared to the NU-BGBM (sRMSE = 0.01833, Time = 96.8399). These results demonstrate the advantages of considering mixed noises and avoiding sparsity terms to improve the accuracy and reduce computational time. A reduction in computational time indicates the feasibility of applying NU-RBGBM as a non-linear unmixing algorithm on large datasets.

## V. CONCLUSION

This paper proposes an augmented version of the bandwise generalised bilinear model based on the maximum a posteriori framework. We employed the ADMM approach for solving the proposed NU-RBGBM. Extensive simulations were performed on synthetic (with simulated mixed noise scenarios) and real HSIs to demonstrate the efficiency of the proposed algorithm. In the synthetic data experiments, the proposed NU-RBGBM has performed better than the other compared methods, specifically in the presence of complex mixed noise. In the real data experiments, NU-RBGBM was able to achieve low sRMSE as compared to other unmixing methods employed in this study.

## VI. REFERENCES


[1] Abderrahim Halimi, Yoann Altmann, Nicolas Dobigeon, and Jean-Yves Tourneret, "Unmixing hyperspectral images using the generalized bilinear model," in *2011 IEEE International Geoscience and Remote Sensing Symposium*. IEEE, 2011, pp. 1886–1889.

[2] Rob Heylen and Paul Scheunders, "A multilinear mixing model for nonlinear spectral unmixing," *IEEE transactions on geoscience and remote sensing*, vol. 54, no. 1, pp. 240–251, 2015.

[3] Bruce Hapke, "Bidirectional reflectance spectroscopy: 1. theory," *Journal of Geophysical Research: Solid Earth*, vol. 86, no. B4, pp. 3039–3054, 1981.

[4] Abderrahim Halimi, Yoann Altmann, Nicolas Dobigeon, and Jean-Yves Tourneret, "Nonlinear unmixing of hyperspectral images using a generalized bilinear model," *IEEE Transactions on Geoscience and Remote Sensing*, vol. 49, no. 11, pp. 4153–4162, 2011.

[5] Hemant Kumar Aggarwal and Angshul Majumdar, "Hyperspectral unmixing in the presence of mixed noise using joint-sparsity and total variation," *IEEE Journal of Selected Topics in Applied Earth Observations and Remote Sensing*, vol. 9, no. 9, pp. 4257–4266, 2016.

[6] Chang Li, Yu Liu, Juan Cheng, Rencheng Song, Hu Peng, Qiang Chen, and Xun Chen, "Hyperspectral unmixing with bandwise generalized bilinear model," *Remote Sensing*, vol. 10, no. 10, pp. 1600, 2018.

[7] José M Bioucas-Dias and Mário AT Figueiredo, "Alternating direction algorithms for constrained sparse regression: Application to hyperspectral unmixing," in *2010 2nd Workshop on Hyperspectral Image and Signal Processing: Evolution in Remote Sensing*. IEEE, 2010, pp. 1–4.

[8] Touseef Ahmad, Rosly Boy Lyngdoh, Anand S Sahadevan, Soumyendu Raha, Praveen K Gupta, and Arundhati Misra, "Four-directional spatial regularization for sparse hyperspectral unmixing," *Journal of Applied Remote Sensing*, vol. 14, no. 4, pp. 046511, 2020.

[9] Fan Fan, Yong Ma, Chang Li, Xiaoguang Mei, Jun Huang, and Jiayi Ma, "Hyperspectral image denoising with superpixel segmentation and low-rank representation," *Information Sciences*, vol. 397, pp. 48–68, 2017.

[10] Marian-Daniel Iordache, José M Bioucas-Dias, and Antonio Plaza, "Sparse unmixing of hyperspectral data," *IEEE Transactions on Geoscience and Remote Sensing*, vol. 49, no. 6, pp. 2014–2039, 2011.

[11] Chang Li, Yong Ma, Xiaoguang Mei, Fan Fan, Jun Huang, and Jiayi Ma, "Sparse unmixing of hyperspectral data with noise level estimation," *Remote Sensing*, vol. 9, no. 11, pp. 1166, 2017.

[12] José MP Nascimento and José M Bioucas-Dias, "Hyperspectral signal subspace estimation," in *2007 IEEE International Geoscience and Remote Sensing Symposium*. IEEE, 2007, pp. 3225–3228.

[13] Stephen Boyd, Neal Parikh, Eric Chu, Borja Peleato, Jonathan Eckstein, et al., "Distributed optimization and statistical learning via the alternating direction method of multipliers," *Foundations and Trends® in Machine learning*, vol. 3, no. 1, pp. 1–122, 2011.

[14] Jonathan Eckstein and Dimitri P Bertsekas, "On the douglas—rachford splitting method and the proximal point algorithm for maximal monotone operators," *Mathematical Programming*, vol. 55, no. 1-3, pp. 293–318, 1992.

[15] Daniel C Heinz et al., "Fully constrained least squares linear spectral mixture analysis method for material quantification in hyperspectral imagery," *IEEE transactions on geoscience and remote sensing*, vol. 39, no. 3, pp. 529–545, 2001.

[16] Naoto Yokoya, Jocelyn Chanussot, and Akira Iwasaki, "Nonlinear unmixing of hyperspectral data using semi-nonnegative matrix factorization," *IEEE Transactions on Geoscience and Remote Sensing*, vol. 52, no. 2, pp. 1430–1437, 2013.

[17] Chang Li, Yong Ma, Jun Huang, Xiaoguang Mei, Chengyin Liu, and Jiayi Ma, "Gbm-based unmixing of hyperspectral data using bound projected optimal gradient method," *IEEE Geoscience and Remote Sensing Letters*, vol. 13, no. 7, pp. 952–956, 2016.

[18] Feiyun Zhu, "Hyperspectral unmixing: ground truth labeling, datasets, benchmark performances and survey," *arXiv preprint arXiv:1708.05125*, 2017.

[19] José MP Nascimento and José MB Dias, "Vertex component analysis: A fast algorithm to unmix hyperspectral data," *IEEE transactions on Geoscience and Remote Sensing*, vol. 43, no. 4, pp. 898–910, 2005.